Theor. Comput. Fluid Dyn.
https://doi.org/10.1007/s00162-024-00713-1

**Lorenzo Fusi · Antonio Giovinetto**

# A spectral collocation scheme for the flow of a piezo-viscous fluid in ducts with slip conditions

Received: 17 April 2024 / Accepted: 5 July 2024


**Abstract** In this paper we present a numerical scheme based on spectral collocation methods to investigate the flow of a piezo-viscous fluid, i.e., a fluid in which the rheological parameters depend on the pressure. In particular, we consider an incompressible Navier–Stokes fluid with pressure dependent viscosity flowing in: (i) a two-dimensional non-symmetric planar channel; (ii) a three-dimensional axisymmetric non-straight conduit. For both cases we impose the Navier slip boundary conditions that can be reduced to the classical no-slip condition for a proper choice of the slip parameter. We assume that the dependence of the viscosity on the pressure is of exponential type (Barus law), even though the model can be replaced by any other viscosity function. We write the mathematical problem (stress based formulation) and discretize the governing equations through a spectral collocation scheme. The advantage of this numerical procedure, which to the authors' knowledge has never been used before for this class of fluids, lies in in the ease of implementation and in the accuracy of the solution. To validate our model we compare the numerical solution with the one that can be obtained in the case of small aspect ratio, i.e., the leading order lubrication solution. We perform some numerical simulation to investigate the effects of the pressure-dependent viscosity on the flow. We consider different wall functions to gain insight also on the role played by the channel/duct geometry. In both cases (i), (ii) we find that the increase of the coefficient appearing in the viscosity function results in a global reduction of the flow, as physically expected.

**Keywords** Pressure dependent viscosity · Poiseuille flow · Navier slip conditions · Spectral collocation methods

## 1 Introduction

Since the seminal work of Bridgman [1] on the physics of high pressure, the interest on fluids with pressure dependent viscosity has constantly grown within the scientific community. Fluids with pressure dependent rheology are ubiquitous in many practical applications, such as geological, environmental, industrial and biological flows. It is well known that the application of high pressure on liquids produces important changes in properties such as compressibility, viscosity, thermal conductivity, etc. The idea that the viscosity of a fluid

Communicated by Soshi Kawai.

Lorenzo Fusi and Antonio Giovinetto have contributed equally to this work.

L. Fusi (✉) · A. Giovinetto
Dipartimento di Matematica e Informatica "Ulisse Dini", Università degli Studi di Firenze, Viale Morgagni 67/a, 50134 Florence, Italy
E-mail: lorenzo.fusi@unifi.it

A. Giovinetto
E-mail: antonio.giovinetto@unifi.it

Published online: 13 July 2024

can depend on pressure was first proposed by Stokes [2]. Subsequently Barus [3] provided an analytical form of the type

$$\mu^* = \mu_o^* \exp(\beta^*(T^*)p^*), \tag{1}$$

where $\mu_o^*$ is a reference viscosity and $\beta^*$ is a coefficient depending on the absolute temperature $T^*$. Another formal expression for the viscosity is the one proposed by Andrade [4], namely

$$\mu^* = Q^* \sqrt{\rho^*} \exp\left[\left(A^* + \rho^{*^2} B^*\right) \frac{C^*}{T^*}\right], \tag{2}$$

where $\rho^*$ is the density and $Q^*$, $A^*$, $B^*$, $C^*$ are constants. Although the increase of the pressure produces an increase of the density, there are cases in which a variation of the pressure does not alter significantly the density but modifies in a dramatic fashion the viscosity, see [5–7]. In these cases we speak of incompressible fluids with pressure dependent viscosity, i.e., of incompressible fluid whose rheology may change with the pressure. Over the past 70 years a remarkable body of experimental evidence has proved the viscosity can depend on the pressure (and temperature), especially when the pressures involved are quite high, see [8–11]. Here we are not interested in a precise form of the function relating the viscosity to the pressure, since we do not deal with a specific application. We however remark that a possible interesting application is the design of lubricants used in journal bearings. It is thus unnecessary to go through a detailed discussion of the experimental studies cited here. It is sufficient to pick up a regular function such as the one proposed by Barus. In practice, we shall consider a Navier–Stokes fluid in which the viscosity depends exponentially on the pressure (piezo-viscous fluid).

The flow of piezo viscous fluids has been extensively studied in the last decades. From the mathematical point of view the dependence of the viscosity on the pressure brings a nonlinearity to the momentum equation that changes the nature of the pressure itself. Indeed, in this case the pressure cannot be eliminated from the system using Helmoltz decomposition and therefore cannot be considered as a Lagrange multiplier. One of the first contributions on existence and uniqueness of solutions for piezo-viscous flows is the one by Renardy [12] for a viscosity function that is sublinear at infinity and whose derivatives are bounded in $\mathbb{R}$. Gazzola et al. [13–15] have proven well posedness results for both the stationary and non-stationary case. An exhaustive treatise on the mathematical properties of piezo-viscous systems is given in [16].

The analytical solutions for these flows have been determined in papers such as [17–25], but only for simple geometries. These analytical solutions are indeed available only in a limited number of geometrical settings and only for the steady state flow, while for more complex situations we must rely on numerical simulations. Some papers have been devoted to the detection of numerical solution and among them we cite [26–28]. It must be said that these works are almost entirely performed in very regular domains (such as straight channels, straight cylindrical annuli and so forth) and, to our knowledge, none of them is based on spectral collocation methods.

In this paper we study the isothermal flow of an incompressible piezo-viscous fluid in a (non necessarily symmetric) duct with Navier slip boundary conditions. The numerical scheme employed here is largely based on the one presented in [29] in which a similar problem was considered for a generalized Newtonian fluid. The mathematical problem consists of a set of nonlinear partial differential equations (stress based formulation) that are discretized and solved via Newton–Raphson algorithm. To validate our model the numerical and analytical solution are compared in the case of a duct with small aspect ratio. Indeed, in this case the analytical solution can be obtained expanding the main variables around the "small parameter" (aspect ratio) and solving the leading order problem. We shall see that the comparison shows an excellent agreement.

We start considering a non-symmetric two-dimensional channel in which the flow is driven by a given pressure gradient. Subsequently we study the three-dimensional flow problem in a non-straight axisymmetric conduit. In both cases the wall boundary conditions are of Navier type, i.e., the wall velocity is proportional to the tangential shear stress.

The numerical solutions will provide the behavior of the velocity field, the pressure field and viscosity. These simulations are important to understand how the flow is affected by the physical parameters appearing in the model and in particular, the Navier slip coefficient and the pressure coefficient.

The constitutive equation of the fluid under examination is

$$\mathbf{T}^* = -p^*\mathbf{I} + \mathbf{S}^*, \quad \mathbf{S}^* = 2\mu^*(p^*)\mathbf{D}^*, \tag{3}$$

where $\mu^*(p^*)$ is a positive smooth function of the pressure $p^*$. In (3) $\mathbf{T}^*$ is the Cauchy stress tensor, $\mathbf{S}^*$ is the traceless part of the stress and $\mathbf{D}^*$ is the symmetric part of the velocity gradient $\mathbf{L}^* = \nabla\mathbf{v}^*$, $\mathbf{v}^* = (u^*, v^*)$

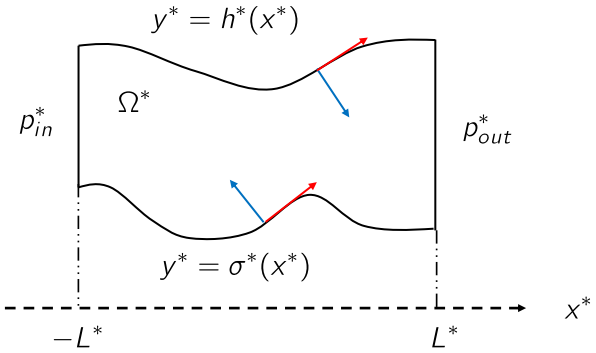


**Fig. 1** Sketch of the domain of the problem. Two dimensional non symmetric channel of non uniform width

being the velocity field. For simplicity we assume that the viscosity function is given by the exponential law

$$\mu^*(p^*) = \mu^*_o \exp\left[\beta^*\left(p^* - p^*_{out}\right)\right], \tag{4}$$

where $\mu^*_o$ is the viscosity at pressure $p^*_{out}$ and $\beta^*$ is a coefficient dimensionally represented as the inverse of a pressure. We remark that our study is not aimed at any specific application, so that, in principle, the exponential formula (4) can be replaced by any smooth positive function of the pressure. On the solid walls we impose the impenetrability and slip conditions

$$\mathbf{v}^* \cdot \mathbf{n} = 0, \quad \left[\alpha^*\left(\mathbf{T}^*\mathbf{n}\right) + \mathbf{v}^*\right] \cdot \mathbf{t} = 0. \tag{5}$$

where $\alpha^*$ is a constant parameter with dimensions $length^2 \cdot time/mass$ (dimensional slip parameter) and where $\mathbf{n}$, $\mathbf{t}$ are the inward normal and tangent unit vectors to the solid walls respectively. Notice that, when $\alpha^* = 0$, we recover the classical no-slip condition at the solid wall. In the absence of body forces, the governing equations are

$$\begin{cases} \rho^* \dot{\mathbf{v}}^* = -\nabla p^* + \nabla \cdot \mathbf{S}^*, \\ \nabla \cdot \mathbf{v}^* = 0, \end{cases} \tag{6}$$

where the first represents the balance of linear momentum and the second represents mass conservation. The superimposed dot in $(6)_1$ represents material differentiation.

## 2 The mathematical model: two dimensional non-symmetric channel

In this section we consider the flow of a piezo-viscous fluid in a non symmetric two-dimensional channel $\Omega^*$ bounded by the edges $x^* = \pm L^*$ and by the solid walls $y^* = h^*(x^*)$, $y^* = \sigma^*(x^*)$, see Fig. 1.
The flow is driven by a constant pressure drop $\Delta p^* = p^*_{in} - p^*_{out} > 0$, where $p^*_{in}$, $p^*_{out}$ are the imposed pressures at $x^* = \pm L^*$. The lateral boundary conditions are $p^* = p^*_{in}$, $v^* = 0$ at $x^* = -L^*$ and $p^* = p^*_{out}$, $v^* = 0$ at $x^* = L^*$. We define

$$H^* = \max_{x^* \in [-L^*, L^*]} \left[\frac{h^*(x^*) - \sigma^*(x^*)}{2}\right], \quad \delta = \frac{H^*}{L^*}, \tag{7}$$

where $H^*$ represents the maximum half width of the channel and $\delta$ is the aspect ratio of the channel. We rescale the variables as:

$$x^* = L^* x, \quad y^* = H^* y, \quad t^* = \left(\frac{L^*}{U^*}\right) t, \quad u^* = U^* u, \tag{8}$$

$$v^* = \delta U^* v, \quad \mu^* = \mu^*_o \mu(p), \quad p^* - p^*_{out} = \left(\frac{\mu^*_o U^*}{\delta H^*}\right) p, \tag{9}$$

$$\mathbf{S}^* = \left(\frac{\mu^*_o U^*}{H^*}\right) \mathbf{S}, \quad \mathbf{D}^* = \left(\frac{U^*}{H^*}\right) \mathbf{D}, \quad \beta^* = \left(\frac{\delta H^*}{\mu^*_o U^*}\right) \beta, \tag{10}$$

where $U^*$ is a characteristic velocity and $\mu(p) = \exp(\beta p)$ is the non dimensional apparent viscosity. The scaled components of the strain-rate tensor $\mathbf{D}$ and of the stress tensor $\mathbf{S}$ are

$$D_{11} = \delta u_x, \quad D_{12} = \frac{1}{2}\big(u_y + \delta^2 v_x\big), \quad D_{22} = \delta v_y, \tag{11}$$

$$S_{11} = 2\delta e^{\beta p} u_x, \quad S_{12} = e^{\beta p}\big(u_y + \delta^2 v_x\big), \quad S_{22} = 2\delta e^{\beta p} v_y, \tag{12}$$

respectively. The non dimensional governing equations are:

$$\begin{cases} \delta Re\dot{u} = -p_x + \delta(S_{11})_x + (S_{12})_y, \\ \delta^3 Re\dot{u} = -p_y + \delta^2(S_{12})_x + \delta(S_{22})_y, \\ u_x + v_y = 0, \end{cases} \tag{13}$$

where $Re = (\rho^* U^* H^*)/\mu_o^*$ is the Reynolds number. The lateral boundary conditions are

$$p = p_{in}, \quad v = 0, \quad \text{on} \quad x = -1, \quad p = 0, \quad v = 0, \quad \text{on} \quad x = 1. \tag{14}$$

where $p_{in} = (\delta \Delta p^* H^*)/(\mu_o^* U^*) > 0$. The impenetrability and slip conditions on $y = h(x)$ become

$$\begin{cases} \alpha\Big[\delta h_x\big(S_{11} - S_{22}\big) - S_{12}\big(1 - \delta^2 h_x^2\big)\Big] + u\big(1 + \delta^2 h_x^2\big)^{\frac{3}{2}} = 0, \\ u h_x - v = 0, \end{cases} \tag{15}$$

while, on $y = \sigma(x)$ we get

$$\begin{cases} \alpha\Big[ - \delta\sigma_x\big(S_{11} - S_{22}\big) + S_{12}\big(1 - \delta^2\sigma_x^2\big)\Big] + u\big(1 + \delta^2\sigma_x^2\big)^{\frac{3}{2}} = 0, \\ -u\sigma_x + v = 0, \end{cases} \tag{16}$$

where $\alpha = (\alpha^* \mu_o^*/H^*)$. The well posedness of problem (13)–(16) is thoroughly discussed in [16].

We make the assumption of creeping flow, i.e., $Re \ll 1$, so that system (13) reduces to

$$\begin{cases} 0 = -p_x + \delta(S_{11})_x + (S_{12})_y, \\ 0 = -p_y + \delta^2(S_{12})_x + \delta(S_{22})_y, \\ u_x + v_y = 0, \end{cases} \tag{17}$$

with boundary conditions (14), (15), (16). From $(15)_2$, $(16)_2$ we notice that whenever $h_x = 0$ or $\sigma_x = 0$ the transversal velocity $v = 0$ on the solid wall. We also notice that, since $v(\pm 1, y) \equiv 0$ on the inlet/outlet, the impenetrability conditions at the four corners $(\pm 1, h(\pm 1))$, $(\pm 1, \sigma(\pm 1))$ imply that

$$u(\pm 1, h(\pm 1))h_x(\pm 1) = v(\pm 1, h(\pm 1)) = 0, \tag{18}$$

$$u(\pm 1, \sigma(\pm 1))\sigma_x(\pm 1) = v(\pm 1, \sigma(\pm 1)) = 0. \tag{19}$$

In general $u \neq 0$ on the solid walls, so we conclude that, in order to have $(15)_2$, $(16)_2$ satisfied up to the four corners of the channel, the wall profiles must be such that $h_x(\pm 1) = \sigma_x(\pm 1) = 0$. In what follows we shall consider solid walls that satisfy this hypothesis.

We notice that the flow rate $Q$ is constant along the channel, since

$$Q = \int_\sigma^h u(x, y)dy, \tag{20}$$

and

$$Q_x = u\Big|_h h_x - u\Big|_\sigma \sigma_x + \int_\sigma^h u_x(x, y)dy, \tag{21}$$

which, because of $(13)_3$, $(15)_2$, $(16)_2$ yields $Q_x = 0$. As a consequence the flow rate is constant throughout the channel.

### 2.1 Analytical solution in the case of small aspect ratio

When $\delta \ll 1$ we may look for a solution written as a power series in $\delta$ and focus on the leading order solution, i.e., the solution of the problem

$$\begin{cases} 0 = -p_x + (S_{12})_y, \quad S_{12} = u_y e^{\beta p}, \\ 0 = -p_y, \\ u_x + v_y = 0. \end{cases} \tag{22}$$

Integrating the momentum equation we find $S_{12} = p_x y + c(x)$, with $c(x)$ unknown. The boundary conditions on the solid walls become

$$\begin{cases} u = \alpha e^{\beta p} u_y, \\ v = u h_x, \end{cases} \quad \text{on} \quad y = h(x), \quad \begin{cases} u = -\alpha e^{\beta p} u_y, \\ v = u \sigma_x, \end{cases} \quad \text{on} \quad y = \sigma(x). \tag{23}$$

The problem is thus symmetric with respect to the curve $y = (h + \sigma)/2$ and $S_{12} = 0$ on such a curve. As a consequence,

$$c(x) = -\frac{p_x}{2}(h + \sigma), \rightarrow u_y = e^{-\beta p} p_x \left[ y - \frac{h + \sigma}{2} \right]. \tag{24}$$

The imposition of the boundary conditions on $y = h$ and $y = \sigma$ leads to

$$u\Big|_h = \frac{\alpha p_x}{2}(h - \sigma), \quad u\Big|_\sigma = \frac{\alpha p_x}{2}(h - \sigma). \tag{25}$$

If we integrate $u_y$ between $y$ and $h$ we find

$$u(x, y) = \frac{\alpha p_x}{2}(h - \sigma) - \frac{p_x e^{-\beta p}}{2}(h - y)(y - \sigma), \tag{26}$$

i.e., the longitudinal component of the velocity at the leading order. Notice that at this stage the pressure is unknown. From the continuity equation we have

$$v\Big|_\sigma - v\Big|_h = u\Big|_\sigma \sigma_x - u\Big|_h h_x = \int_\sigma^h -v_y dy = \int_\sigma^h u_x dy. \tag{27}$$

We now differentiate (26) with respect to $x$ and substitute in the last integral of (27). Inserting (25) into (27) and integrating we find

$$\frac{d}{dx}\left\{ p_x \left[ 6\alpha(h - \sigma)^2 - e^{-\beta p}(h - \sigma)^3 \right] \right\} = 0, \tag{28}$$

which is a second order differential equation for the pressure $p$. Equation (28) plus the boundary conditions $p(-1) = p_{in}$, $p(1) = 0$ provides the BVP for the pressure, namely

$$\begin{cases} p_{xx} = -p_x \dfrac{\left[ 6\alpha(h - \sigma)^2 - e^{-\beta p}(h - \sigma)^3 \right]_x}{\left[ 6\alpha(h - \sigma)^2 - e^{-\beta p}(h - \sigma)^3 \right]}, \\ p(-1) = p_{in}, \quad p(1) = 0. \end{cases} \tag{29}$$

Once (29) is solved, and this can be done only numerically, the pressure gradient $p_x$ can be substituted in (26) providing the longitudinal velocity $u$. The transversal component $v$ of the velocity is then obtained from

$$v\Big|_y - v\Big|_h = \int_y^h -v_y dy = \int_y^h u_x dy. \tag{30}$$

After some calculations we find

$$v(x, y) = \frac{\partial}{\partial x}\left[ \frac{\alpha p_x}{2}(h - \sigma)(h - y) + \frac{p_x e^{-\beta p}}{12}(h - y)^2(3\sigma - 2y - h) \right]. \tag{31}$$

From (28) we see that

$$p_x \left[ 6\alpha(h - \sigma)^2 - e^{-\beta p}(h - \sigma)^3 \right] = const. \tag{32}$$

Hence, when $\alpha = 0$ we find

$$-p_x e^{-\beta p} = \frac{const}{(h-\sigma)^3}, \quad v(x,y) = -\frac{\partial}{\partial x}\left[\frac{(h-y)^2(3\sigma-2y-h)}{12(h-\sigma)^3}\right], \tag{33}$$

implying

$$v(x,y) = \frac{\partial}{\partial x}\Big[\mathcal{F}(h,\sigma,y)\Big] = \mathcal{F}_h h_x + \mathcal{F}_\sigma \sigma_x. \tag{34}$$

Hence, if there exists some $\bar{x}$ such that $h_x = \sigma_x = 0$, then $v(\bar{x}, y) \equiv 0$. On the other hand, when $\beta = 0$ (Newtonian fluid)

$$p_x\big[6\alpha(h-\sigma)^2 - (h-\sigma)^3\big] = const, \rightarrow p_x = \mathcal{G}(h,\sigma), \tag{35}$$

and

$$v(x,y) = \frac{\partial}{\partial x}\left[\frac{\alpha p_x}{2}(h-\sigma)(h-y) + \frac{p_x}{12}(h-y)^2(3\sigma-2y-h)\right]. \tag{36}$$

Therefore, once again, we find

$$v(x,y) = \frac{\partial}{\partial x}\Big[\mathcal{H}(h,\sigma,y)\Big] = \mathcal{H}_h h_x + \mathcal{H}_\sigma \sigma_x, \tag{37}$$

and $v \equiv 0$ at each $\bar{x}$ such that $h_x = \sigma_x = 0$.

## 2.2 The numerical scheme

In this section we show how to solve problem (17) numerically by means of a spectral collocation scheme. As a first step we must transform the physical domain $\Omega$ in the computational domain $[-1,1]^2$. To this aim we consider the mappings

$$\begin{cases} \xi = x, \\ \eta = \dfrac{2y-(h+\sigma)}{(h-\sigma)}, \end{cases} \quad \begin{cases} x = \xi, \\ y = \dfrac{1}{2}\Big[(h+\sigma)+\eta(h-\sigma)\Big]. \end{cases} \tag{38}$$

The coordinates $(\xi,\eta) \in [-1,1]^2$ are the computational coordinates. For any given function $\phi$, we denote with $\hat{\phi}$ the function with respect to the variables $(\xi,\eta)$, i.e., $\phi(x,y) = \hat{\phi}(\xi,\eta)$. It is easy to express the spatial derivatives with respect to the new variables

$$P_1 := \frac{\partial}{\partial x} = \frac{\partial}{\partial \xi} - \left[\frac{\eta(\hat{h}_\xi - \hat{\sigma}_\xi) + (\hat{h}_\xi + \hat{\sigma}_\xi)}{(\hat{h}-\hat{\sigma})}\right]\frac{\partial}{\partial \eta}, \tag{39}$$

$$P_2 := \frac{\partial}{\partial y} = \frac{2}{(\hat{h}-\hat{\sigma})}\frac{\partial}{\partial \eta}. \tag{40}$$

The problem (17) can be reformulated in the new coordinate system $(\xi,\eta)$ for the vector function $\hat{\mathbf{X}} = (\hat{S}_{11}, \hat{S}_{12}, \hat{S}_{22}, \hat{u}, \hat{v}, \hat{p})^T$.

$$\begin{bmatrix} \delta P_1 & P_2 & 0 & 0 & 0 & -P_1 \\ 0 & \delta^2 P_1 & \delta P_2 & 0 & 0 & -P_2 \\ 1 & 0 & 0 & -2\delta e^{\beta\hat{p}} P_1 & 0 & 0 \\ 0 & 1 & 0 & -e^{\beta\hat{p}} P_2 & -\delta^2 e^{\beta\hat{p}} P_1 & 0 \\ 0 & 0 & 1 & 0 & -2\delta e^{\beta\hat{p}} P_2 & 0 \\ 0 & 0 & 0 & P_1 & P_2 & 0 \end{bmatrix} \begin{bmatrix} \widehat{S}_{11} \\ \widehat{S}_{12} \\ \widehat{S}_{22} \\ \widehat{u} \\ \widehat{v} \\ \widehat{p} \end{bmatrix} = 0, \tag{41}$$

to which we must add the boundary conditions

$$\begin{bmatrix} \delta\alpha\hat{h}_\xi & -\alpha(1-\delta^2\hat{h}_\xi^2) & -\delta\alpha\hat{h}_\xi & (1+\delta^2\hat{h}_\xi^2)^{(3/2)} & 0 & 0 \\ 0 & 0 & 0 & \hat{h}_\xi & -1 & 0 \end{bmatrix} \hat{\mathbf{X}} = 0, \quad \text{on} \quad \eta = 1, \tag{42}$$

**Table 1** Norm (48) representing the absolute error between the numerical and analytical solution. $N = 20$, $\alpha = -1$ and $\beta = 1$

| $\epsilon(\delta)$ | $\delta$ |
|---|---|
| 1.641076333340799 | 1 |
| 0.349446431546098 | 0.5 |
| 0.013604396600548 | 0.1 |
| 0.003368633037444 | 0.05 |
| $5.450549014254116 \cdot 10^{-4}$ | 0.01 |
| $3.444601416401797 \cdot 10^{-5}$ | 0.001 |

$$\begin{bmatrix} -\delta\alpha\hat{\sigma}_\xi & \alpha(1-\delta^2\hat{\sigma}_\xi^2) & -\delta\alpha\hat{\sigma}_\xi & (1+\delta^2\hat{\sigma}_\xi^2)^{(3/2)} & 0 & 0 \\ 0 & 0 & 0 & -\hat{\sigma}_\xi & 1 & 0 \end{bmatrix} \hat{\mathbf{X}} = 0, \quad \text{on} \quad \eta = -1, \tag{43}$$

and

$$\hat{p} = p_{in}, \quad \hat{v} = 0 \quad \text{on} \quad \xi = -1, \quad \hat{p} = \hat{v} = 0 \quad \text{on} \quad \xi = 1. \tag{44}$$

Problem (41) with BCs (42)–(44) is discretized as in [29] producing an overdetermined non-square nonlinear system

$$\mathbf{F}(\hat{\mathbf{X}}) = \mathbf{0}, \tag{45}$$

that is solved via Newton–Raphson algorithm

$$\left[\mathbf{J}(\hat{\mathbf{X}}^n)\right]\Delta\hat{\mathbf{X}}^n = -\mathbf{F}(\hat{\mathbf{X}}^n), \quad \hat{\mathbf{X}}^{n+1} = \hat{\mathbf{X}}^n + \Delta\hat{\mathbf{X}}^n, \tag{46}$$

where $\mathbf{J}(\hat{\mathbf{X}}^n)$ is the Jacobian of $\mathbf{F}(\hat{\mathbf{X}})$ evaluated at iteration $n$. The matrix $\mathbf{J}(\hat{\mathbf{X}}^n)$ is not square and $\Delta\hat{\mathbf{X}}^n$ is a least-square solution of $(46)_1$.

### 2.3 Numerical results and discussion: non-symmetric channel

In this section we present some numerical simulations with the aim of studying the behavior of the main physical variables of the problem. The number of Gauss–Lobatto points for the numerical grid is taken $N = 20$, as in [29]. We have chosen this number because for $N > 20$ the variation of the sup norm of the solution is at the sixth decimal digit (this is due to the high accuracy of the spectral collocation method). The average runtime of the simulations is less than 30 s and the implementation of the numerical codes has been performed in Matlab. We shall consider some general wall functions $h(x)$, $\sigma(x)$ and various values of the parameters $\alpha$, $\beta$ and $\delta$. We begin by taking

$$h(x) = \frac{9}{10} + \frac{1}{10}\cos\left(\frac{\pi}{2}(x+1)\right), \quad \sigma(x) = \frac{3}{10} + \frac{2}{10}\cos\left(\frac{\pi}{2}(x+1)\right), \tag{47}$$

i.e., a non symmetric channel satisfying the compatibility conditions $h_x(\pm 1) = \sigma_x(\pm 1) = 0$. First of all we validate our numerical scheme with the analytical solution determined in Sect. 2.1 which is valid when the aspect ratio of the channel $\delta$ is small. To this aim we consider the sup norm

$$\epsilon(\delta) = \|(u_N, v_N, p_N) - (u, v, p)\|_\infty, \tag{48}$$

where $(u_N, v_N, p_N)$ is the numerical solution and $(u, v, p)$ is the analytical solution determined in Sect. 2.1. The function $\epsilon(\delta)$ defined in (48) clearly makes sense only for small values of $\delta$. We take $\alpha = -1$, $\beta = 1$, but any other value for the two parameters could be used. In Table 1 we show the values of $\epsilon$ for decreasing $\delta$. As expected $\epsilon$ decrease for decreasing $\delta$, showing the validity of our numerical scheme.

Let us now perform some numerical simulations to investigate the behavior of the numerical solution for different values of the physical parameters involved in the model and for various wall profiles. For these numerical simulations we take $\delta = 1$, i.e., a channel whose characteristic length is equal to the characteristic half width. In Figs. 2, 3, 4 and 5 we show the 3D plots of the velocity components, of the pressure and of the apparent viscosity for $\alpha = -1$, $\beta = 1$ and $\delta = 1$ and for the channel profile (47). On the $(x, y, 0)$ plane we have also plotted the wall profiles (dashed line). We observe that the longitudinal velocity is larger in the narrow part of the channel and that the apparent viscosity diminishes along the channel because of the decrease

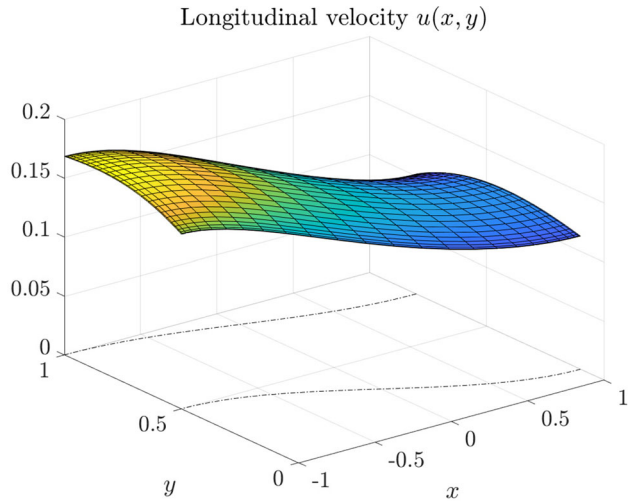


**Fig. 2** Wall profiles (47). Velocity $u(x, y)$, $\alpha = -1$, $\beta = 1$, $\delta = 1$

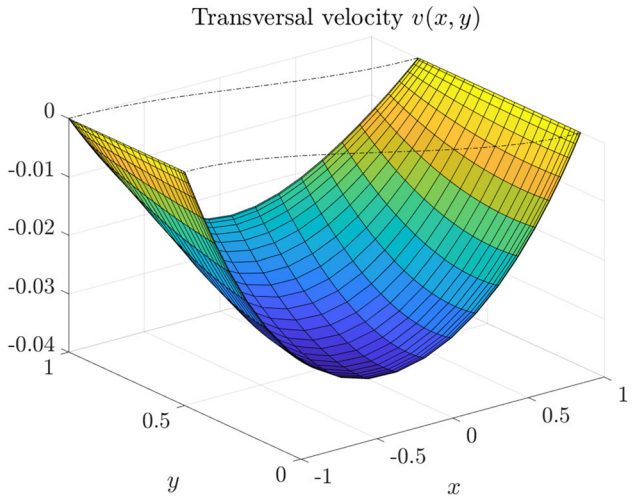


**Fig. 3** Wall profiles (47). Velocity $v(x, y)$, $\alpha = -1$, $\beta = 1$, $\delta = 1$

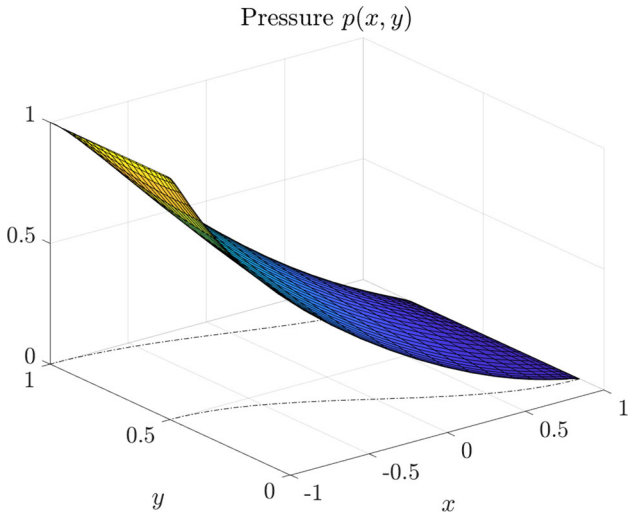


**Fig. 4** Wall profiles (47). Pressure $p(x, y)$, $\alpha = -1$, $\beta = 1$, $\delta = 1$

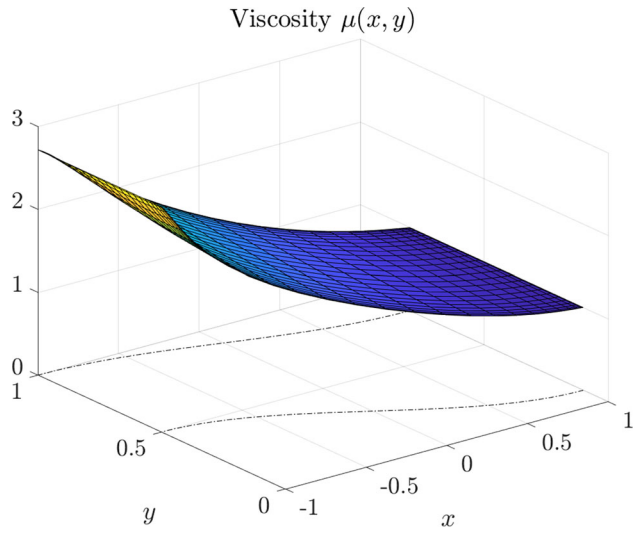


**Fig. 5** Wall profiles (47). Viscosity $\mu(x, y)$, $\alpha = -1$, $\beta = 1$, $\delta = 1$

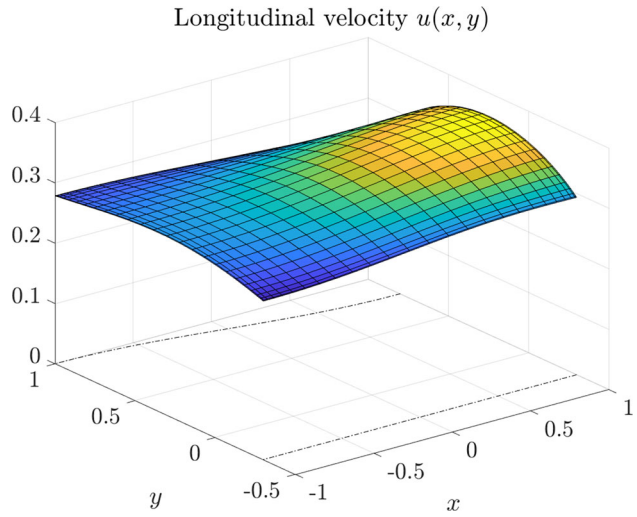


**Fig. 6** Wall profiles (49). Velocity $u(x, y)$, $\alpha = -1$, $\beta = 1$, $\delta = 1$

of the pressure. One can easily check that the boundary conditions at the inlet/outlet (14) and the compatibility conditions (18), (19) are satisfied.

Let us now consider the wall profiles

$$h(x) = \frac{9}{10} + \frac{1}{10}\cos\left(\frac{\pi}{2}(x+1)\right), \quad \sigma(x) \equiv -0.3, \tag{49}$$

with $\alpha = -1$, $\beta = 1$ and $\delta = 1$. The 3D plots for $u$, $v$, $p$ and $\mu$ are shown in Figs. 6, 7, 8 and 9.

Once again, we notice that the longitudinal velocity is larger in the narrow part of the channel, that is in the final section of the channel where the pressure is smaller. This result shows that the increase of the longitudinal velocity is not due to the increase of the pressure but only to the shrinking of the channel gap, since in the last part of the channel the pressure $p$ is reduced whereas $u$ increases. The apparent viscosity follows the behavior of the pressure, since $\mu$ is an increasing function of the pressure ($\beta > 0$). We also see that the transversal velocity $v \equiv 0$ on $y = \sigma$, since $\sigma_x \equiv 0$, see the boundary conditions $(16)_2$. Differently from the case in which the channel walls are given by (47), here the pressure and the apparent viscosity are not monotone in $x$ in the proximity of the upper wall. This last result shows that the monotonicity of the pressure is strictly influenced by the geometry of the channel.

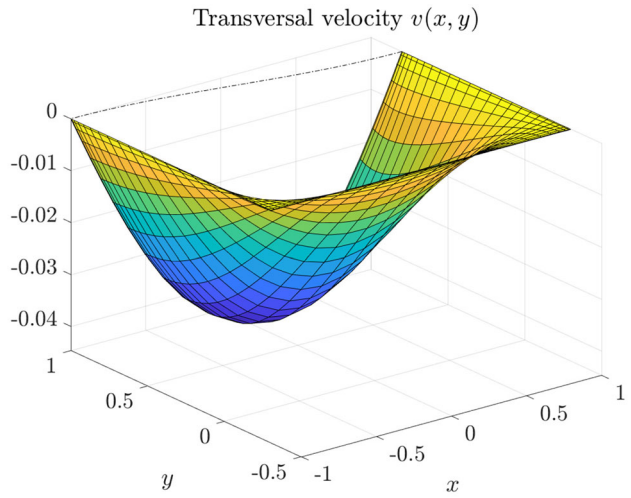


**Fig. 7** Wall profiles (49). Velocity $v(x, y)$, $\alpha = -1$, $\beta = 1$, $\delta = 1$

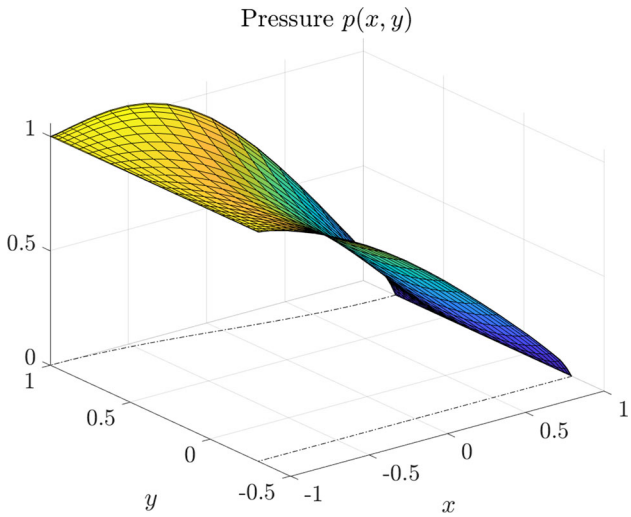


**Fig. 8** Wall profiles (49). Pressure $p(x, y)$, $\alpha = -1$, $\beta = 1$, $\delta = 1$

Let us now pass to investigate the effects of the parameters $\alpha$ and $\beta$ on the solution of the problem. We begin by considering the case of fixed $\alpha$ and variable $\beta$, i.e., a changing apparent viscosity. In Figs. 10, 11, 12 and 13 we plot the variables $u$, $v$, $p$, $\mu$ for wall functions (47) with $\alpha = -1$, $\delta = 1$ and $\beta = -1, 0, 1$. Looking at Figs. 10 and 11, we immediately observe that the velocity components $u$, $v$ decrease (in modulus) with $\beta$. This is physically consistent, since a small value of $\beta$ is characteristic of a "less viscous" fluid, i.e., a fluid that flows "more easily" and hence "more rapidly". The pressure distribution does not show significant variations for the three values of $\beta$ considered, even though it seems to be a bit larger for smaller values of $\beta$ (this behavior is inverted in the proximity of the channel corners, see Fig. 12). The apparent viscosity is strongly influenced by the parameter $\beta$ and $\mu$ increases with $\beta$, as expected, see Fig. 13. From this plot it is evident how the deviation from the Newtonian model (corresponding to $\beta = 0$) alters the flow properties of the fluid. In particular, it is evident that, for fixed value of $\alpha$ and $p_{in}$ and for a viscosity function which grows with pressure, the flow is slower than in the Newtonian case.

Let us now consider the case in which $\beta$ is kept fixed and $\alpha$ varies. This situation is representative of different types of channel walls, i.e., different slip conditions. In Figs. 14, 15, 16 and 17 we plot the variables $u$, $v$, $p$, $\mu$ for wall profiles (47) with $\beta = 1$, $\delta = 1$ and $\alpha = -2, -1, 0$. The increase (in modulus) of the slip parameter $\alpha$ induces an increase of the velocity components (in modulus). This is physically consistent, since the resistance exerted by the solid walls is reduced when $|\alpha|$ is increased and the fluid flows more easily.

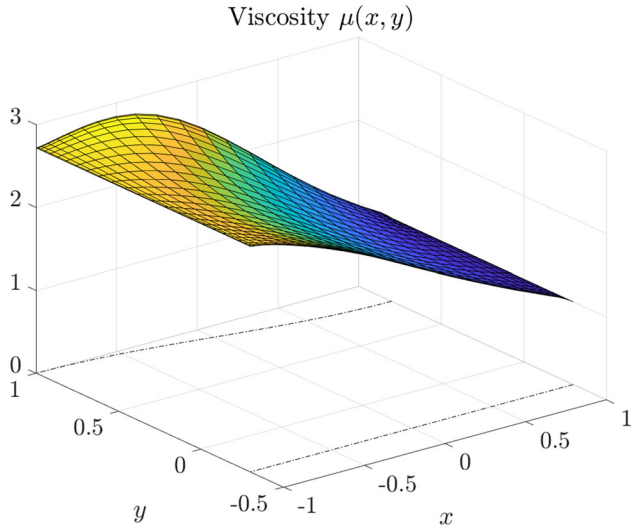


**Fig. 9** Wall profiles (49). Viscosity $\mu(x, y)$, $\alpha = -1$, $\beta = 1$, $\delta = 1$

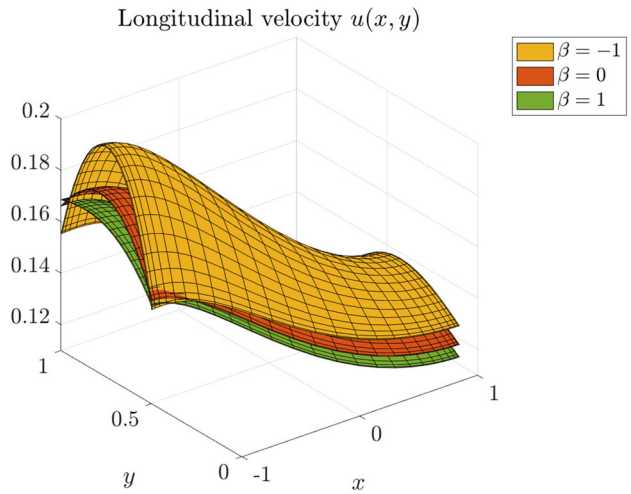


**Fig. 10** Wall profiles (47). Velocity $u(x, y)$, $\alpha = -1$, $\delta = 1$, $\beta = -1, 0, 1$

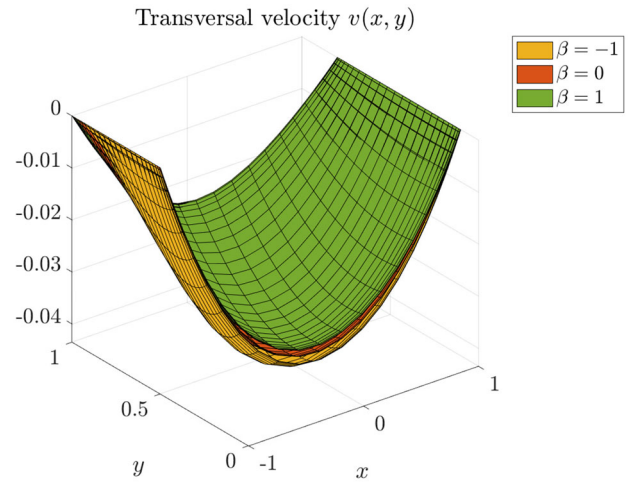


**Fig. 11** Wall profiles (47). Velocity $v(x, y)$, $\alpha = -1$, $\delta = 1$, $\beta = -1, 0, 1$

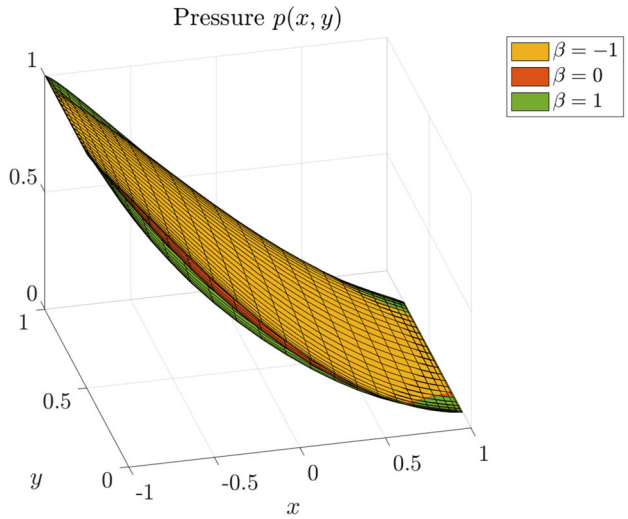


**Fig. 12** Wall profiles (47). Pressure $p(x, y)$, $\alpha = -1$, $\delta = 1$, $\beta = -1, 0, 1$

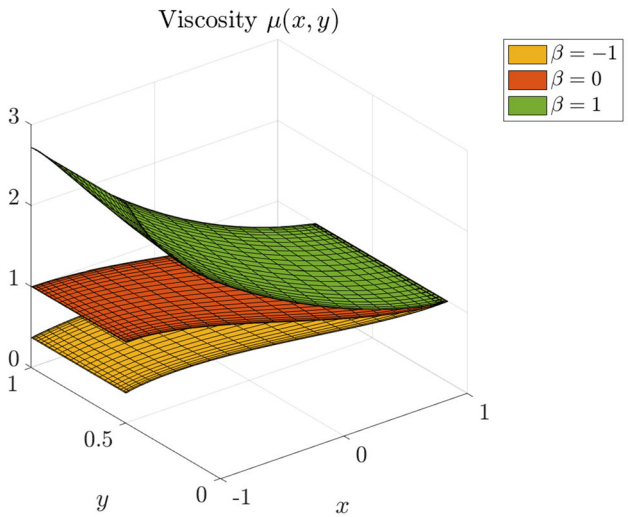


**Fig. 13** Wall profiles (47). Viscosity $\mu(x, y)$, $\alpha = -1$, $\delta = 1$, $\beta = -1, 0, 1$

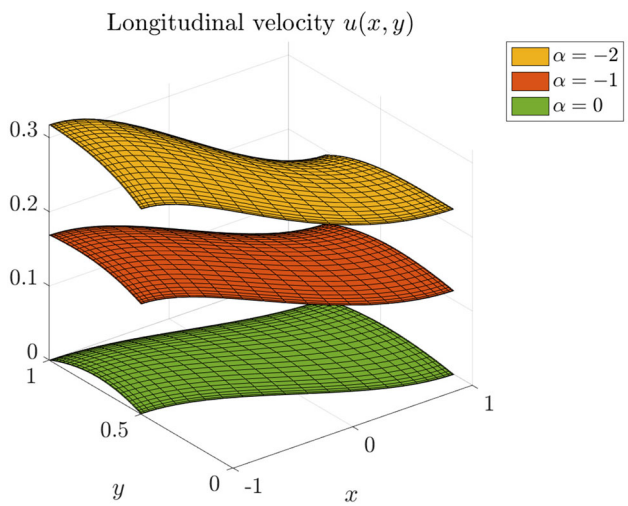


**Fig. 14** Wall profiles (47). Velocity $u(x, y)$, $\beta = 1$, $\delta = 1$, $\alpha = -2, -1, 0$

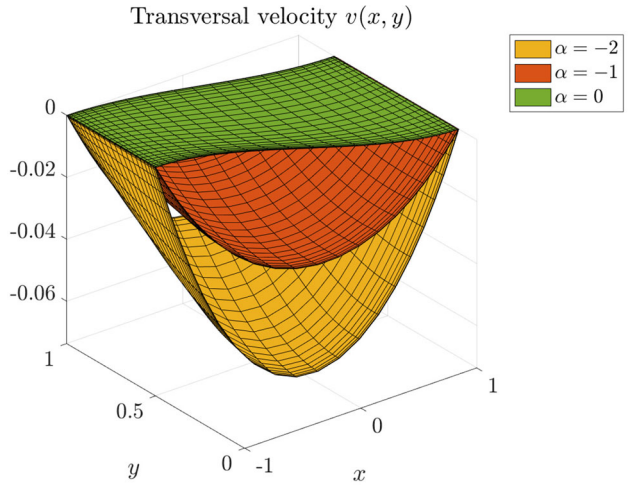


**Fig. 15** Wall profiles (47). Velocity $v(x, y)$, $\beta = 1, \delta = 1, \alpha = -2, -1, 0$

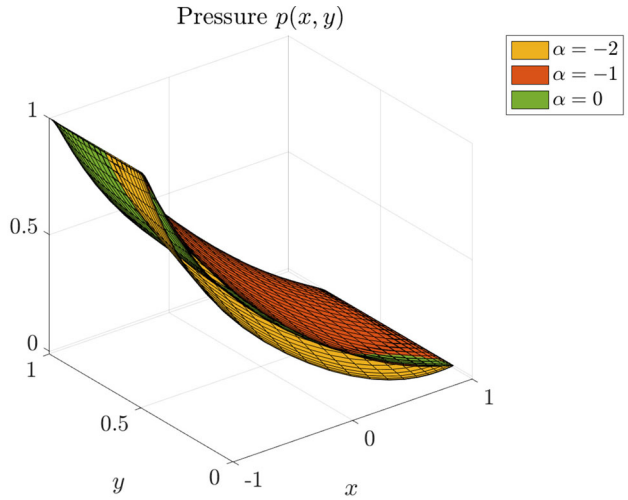


**Fig. 16** Wall profiles (47). Pressure $p(x, y)$, $\beta = 1, \delta = 1, \alpha = -2, -1, 0$

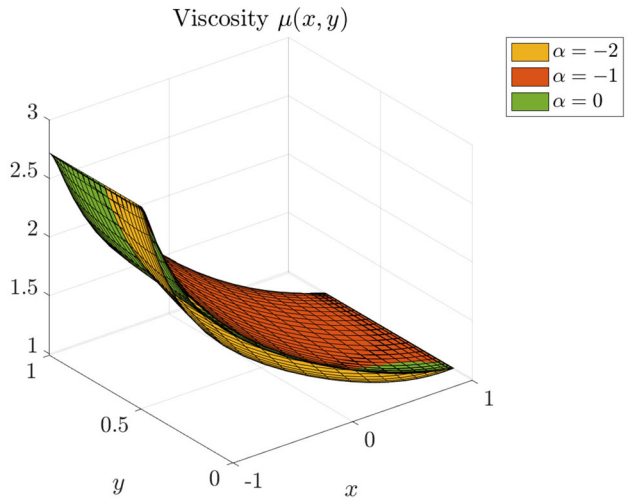


**Fig. 17** Wall profiles (47). Viscosity $\mu(x, y)$, $\beta = 1, \delta = 1, \alpha = -2, -1, 0$

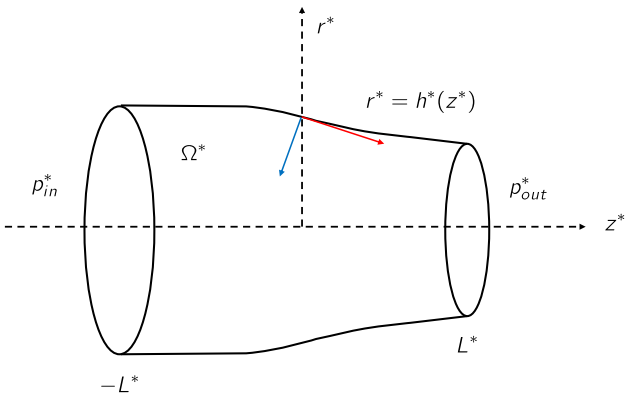


**Fig. 18** Sketch of the domain of the problem. Cylindrical axisymmetric channel of non constant radius $r^* = h^*(z^*)$

The pressure, and hence the viscosity, seems to be less affected by the value of $\alpha$. Indeed, looking at Figs. 16 and 17, we notice that the pressure and the apparent viscosity do not show significant changes for increasing $|\alpha|$ and that there are regions in which the three surfaces corresponding to the different values of $\alpha$ overlap.

## 3 Flow in an axisymmetric cylindrical channel with slip conditions

Let us consider the flow of a piezo-viscous fluid in a axisymmetric tube of non constant radius $r^* = h^*(z^*)$ and length $2L^*$, like the one depicted in Fig. 18.

Because of symmetry, the steady state velocity field in the cylindrical coordinates system $(r^*, \theta, z^*)$ acquires the form $\mathbf{v}^*(r^*, z^*) = v^*(r^*, z^*)\mathbf{e}_r + w^*(r^*, z^*)\mathbf{e}_z$. The only non zero components of the deviatoric stress $\mathbf{S}^*$ defined in (3) are

$$S^*_{rr} = 2\mu^* v^*_r, \quad S^*_{\theta\theta} = \frac{2\mu^* v^*}{r^*}, \quad S^*_{rz} = \mu^*(w^*_r + v^*_z), \quad S^*_{zz} = 2\mu^* w^*_z. \tag{50}$$

We define $R^* = \max h^*(z^*)$ and $\delta = R^*/L^*$. The variables $r^*$, $z^*$, $v^*$ and $w^*$ are scaled with $R^*$, $L^*$, $U^*$, $\delta U^*$, respectively. The pressure, stress and symmetric part of the velocity gradient are scaled as in (8), (10) (with $H^*$ replaced by $R^*$). In the hypothesis of creeping flow, the system of non-dimensional governing equations is given by

$$\begin{cases} 0 = -rp_r + \delta r\big(S_{rr}\big)_r + \delta\big(S_{rr} - S_{\theta\theta}\big) + \delta^2 r\big(S_{rz}\big)_z, \\ 0 = -rp_z + S_{rz} + r\big(S_{rz}\big)_r + \delta r\big(S_{zz}\big)_z, \\ \big(rv\big)_r + rw_z = 0, \\ S_{rr} = 2\mu\delta v_r, \quad S_{rz} = \mu\big(w_r + \delta^2 v_z\big), \\ S_{\theta\theta} = 2\mu v/r, \quad S_{zz} = 2\mu\delta w_z. \end{cases} \tag{51}$$

The non dimensional boundary conditions are now given by

$$p = p_{in}, \quad v = 0, \quad \text{on} \quad z = -1, \quad p = 0, \quad v = 0, \quad \text{on} \quad z = 1, \tag{52}$$

$$\begin{cases} \alpha\Big[\delta h_z\big(S_{zz} - S_{rr}\big) - S_{rz}\big(1 - \delta^2 h_z^2\big)\Big] + w\big(1 + \delta^2 h_z^2\big)^{\frac{3}{2}} = 0, \\ wh_z - v = 0, \end{cases} \tag{53}$$

on $r = h(z)$ and

$$w_r = 0, \quad v = 0, \quad \text{on} \quad r = 0, \quad \text{(symmetry)}. \tag{54}$$

The well posedness of problem (51)–(54) is proven in [16]. Proceeding as in Sect. 2.1, we can prove that the leading order solution of the lubrication flow $\delta \ll 1$ is given by (we skip all the calculation because they are very similar to those of Sect. 2.1)

$$u(r, z) = \frac{\alpha p_z h}{2} + \frac{p_z e^{-\beta p}}{4}(r^2 - h^2), \tag{55}$$

**Table 2** Norm (48) representing the absolute error between the numerical and analytical solution

| $\epsilon(\delta)$ | $\delta$ |
|---|---|
| 3.624850411161941 | 1 |
| 0.865293190703391 | 0.5 |
| 0.034789099947078 | 0.1 |
| 0.009016829486871 | 0.05 |
| 0.002197874463444 | 0.01 |
| $1.984851997393461 \cdot 10^{-4}$ | 0.001 |

$N = 20, \alpha = -1$ and $\beta = 1$

$$v(r,z) = -\frac{\partial}{\partial z}\left[\frac{\alpha p_z h}{4} + \frac{p_z e^{-\beta p}}{16}(r^3 - 2h^2 r)\right], \tag{56}$$

where $p = p(z)$ is the solution of the second order BVP

$$\begin{cases} p_{zz} = -p_z \dfrac{\left[4\alpha h^3 - e^{-\beta p} h^4\right]_z}{\left[4\alpha h^3 - e^{-\beta p} h^4\right]}, \\ p(-1) = p_{in}, \quad p(1) = 0. \end{cases} \tag{57}$$

We remark that also in the cylindrical case the flow rate is constant along the tube. The proof is analogous to that given for the planar case at the end of Sect. 2.

### 3.1 Numerical results and discussion: axisymmetric conduit

In this section we present the numerical simulations for the system (51), (52), (53), (54) obtained, once again, with the use of a spectral collocation scheme analogous to the one of Sect. 2.2 (we skip all the details that are similar to those of the planar case). The number of Gauss–Lobatto points for the numerical grid is still $N = 20$. We consider the wall function

$$h(z) = \frac{9}{10} + \frac{1}{10}\cos\left(\frac{\pi}{2}(z+1)\right), \tag{58}$$

which satisfy the compatibility condition $h_z(\pm 1) = 0$. We validate our model, comparing the numerical solution with the analytical solution in the case $\delta < 1$. Recalling the definition of $\epsilon(\delta)$ given in (48) we obtain the sequence shown in Table 2, proving the validity of our numerical scheme. In Figs. 19, 20, 21 and 22 we plot the velocity components, pressure and apparent viscosity for $\delta = 1$, $\alpha = -1$ and $\beta = 1$. We notice that the longitudinal component increases in the narrow part of the channel, as observed for the planar case. One can easily notice that the overall behavior of the solution is very similar to that of the planar case, as expected.

We then consider a wall function that is not monotone, namely

$$h(z) = 1 - \frac{1}{5}(z^2 - 1)^2. \tag{59}$$

The solution for the profile 59 with $\delta = 1$, $\alpha = -1$ and $\beta = 1$ is depicted in Figs. 23, 24, 25 and 26.

Once again we notice how the pressure (and consequently the apparent viscosity) is influenced by the geometry of the channel.

In Figs. 27, 28, 29 and 30 we show the effects of the pressure coefficient $\beta$ on the solution with wall function (59). We again observe that, as $\beta$ increases the flow is slowed down because of the increase of viscosity (larger flow resistance).

In Figs. 31, 32, 33 and 34 we show the effects of the slip coefficient $\alpha$ on the solution with wall function (59).

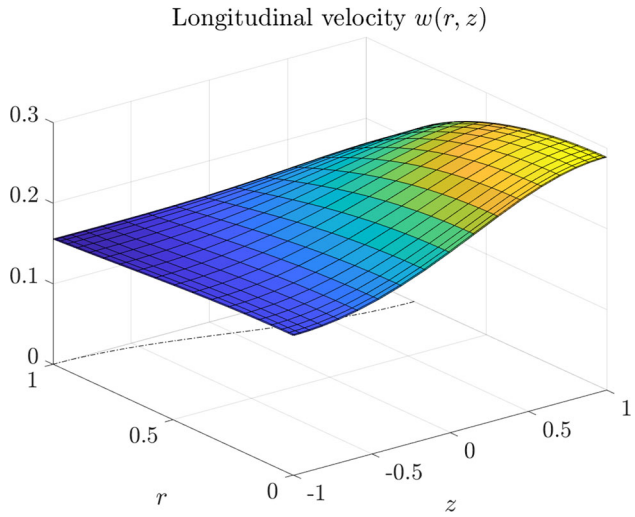


**Fig. 19** Wall profiles (58). Velocity $u(r,z)$, $\beta = 1$, $\delta = 1$, $\alpha = -1$

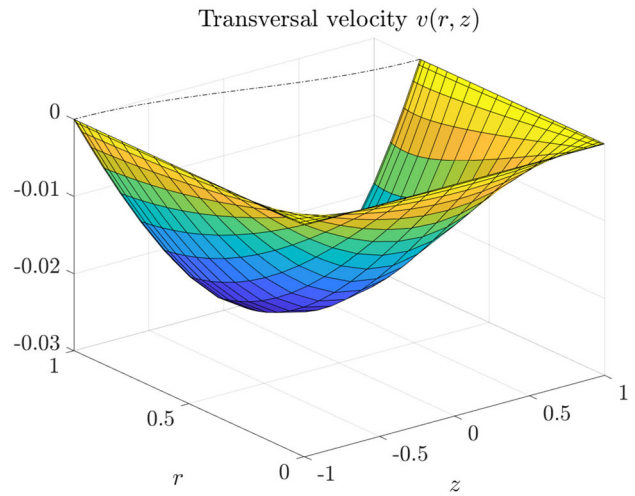


**Fig. 20** Wall profiles (58). Velocity $v(r,z)$, $\beta = 1$, $\delta = 1$, $\alpha = -1$

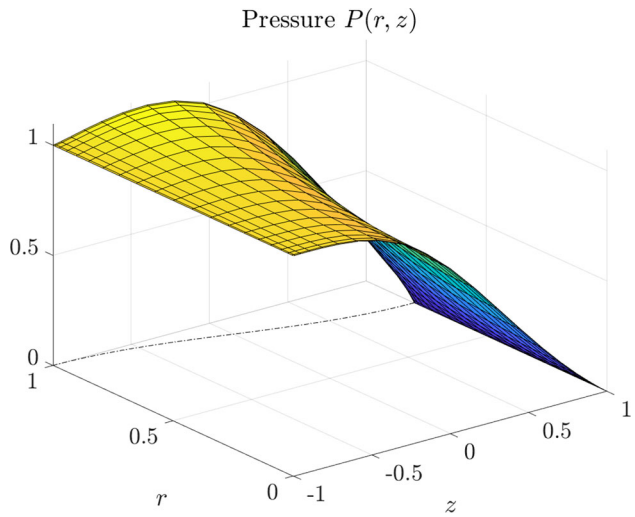


**Fig. 21** Wall profiles (58). Pressure $p(r,z)$, $\beta = 1$, $\delta = 1$, $\alpha = -1$

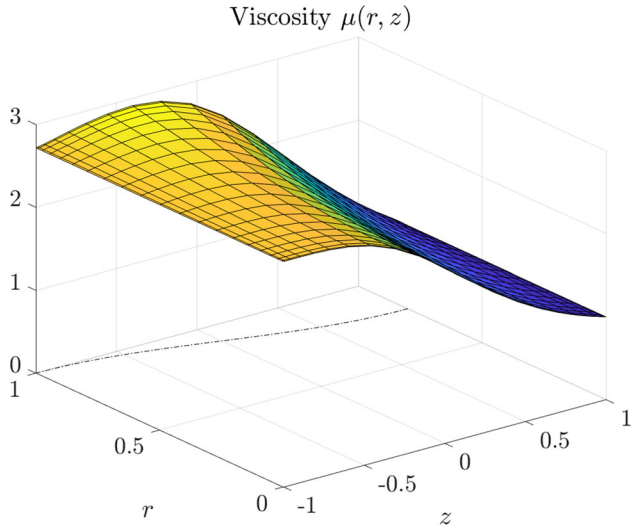


**Fig. 22** Wall profiles (58). Viscosity $\mu(r,z)$, $\beta=1$, $\delta=1$, $\alpha=-1$

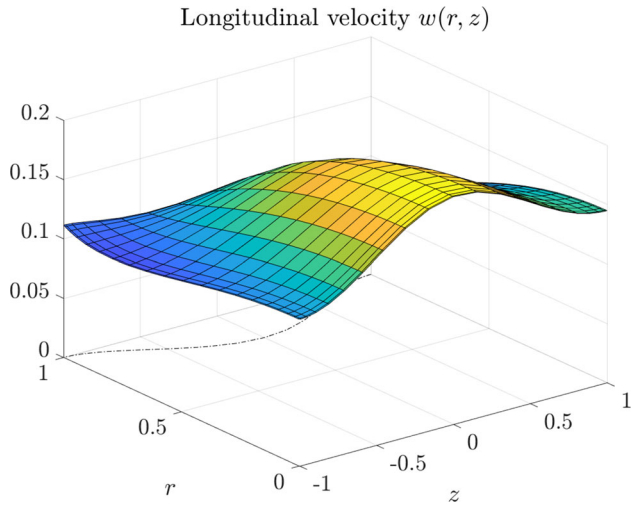


**Fig. 23** Wall profiles (59). Velocity $u(r,z)$, $\beta=1$, $\delta=1$, $\alpha=-1$

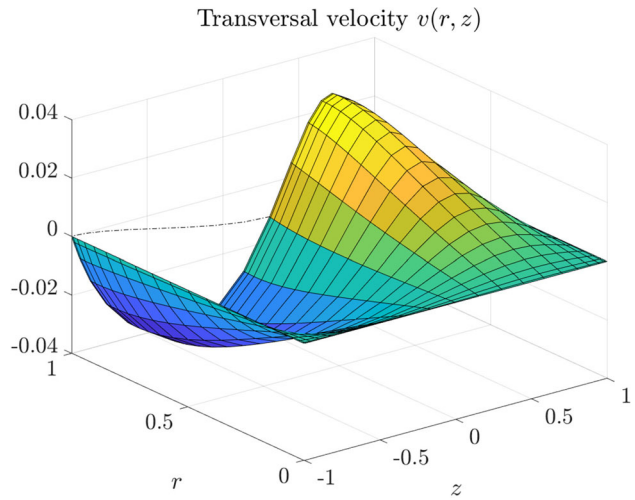


**Fig. 24** Wall profiles (59). Velocity $v(r,z)$, $\beta=1$, $\delta=1$, $\alpha=-1$

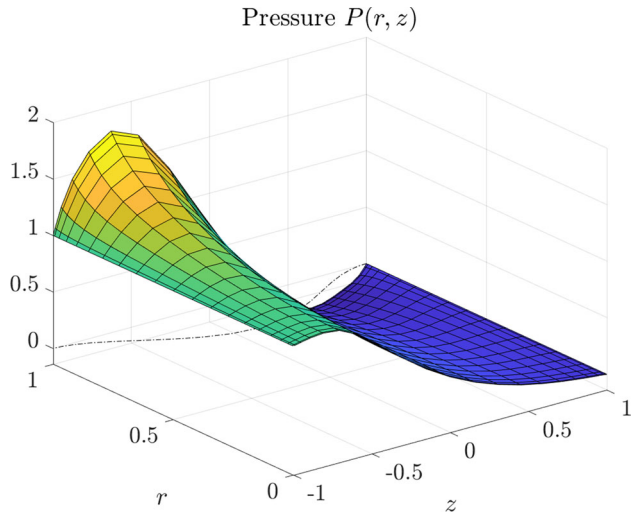


**Fig. 25** Wall profiles (59). Pressure $p(r, z)$, $\beta = 1$, $\delta = 1$, $\alpha = -1$

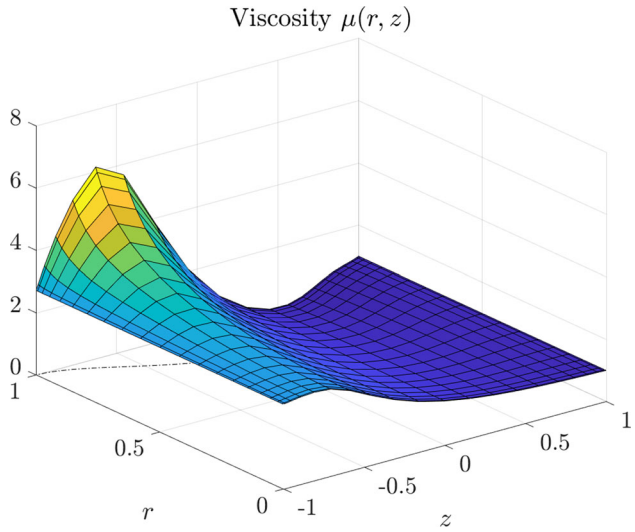


**Fig. 26** Wall profiles (59). Viscosity $\mu(r, z)$, $\alpha = -1$, $\delta = 1$, $\beta = -1, 0, 1$

## 4 Conclusions and perspectives

We have presented a numerical scheme based on spectral collocation methods to study the flow of a piezo-viscous fluid in a non symmetric non-straight channel and in an axisymmetric non-straight pipe. The mathematical problem, reformulated with non-dimensional variables and discretized through a spectral collocation scheme, consists in a set of non linear partial differential and algebraic equations to which we have added Navier slip conditions at the walls and inlet/outlet boundary conditions. We have assumed that the viscosity depends on the pressure in an exponential way, even if other choices are clearly possible. We have performed a series of numerical simulations for different wall functions and different values of the rheological parameters appearing in the model. We have validated our numerical scheme through a comparison of the numerical solution with the analytical solution that one can obtain in the case of small aspect ratio, i.e., the leading order lubrication solution. This comparison has shown an excellent agreement. We have shown that the flow is strongly influenced by the coefficient $\beta$ (pressure coefficient) that relates the viscosity to the pressure in the viscosity function. To highlight the effects due to the dependence of the viscosity on the pressure, we have compared the numerical results of the piezo-viscous flow with the Newtonian case. We have shown that the increase of $\beta$ results in a global reduction of the flow, essentially due to the increase of the apparent viscosity. We have observed that the flow is also influenced by the slip coefficient $\alpha$ and by the geometry of the system.

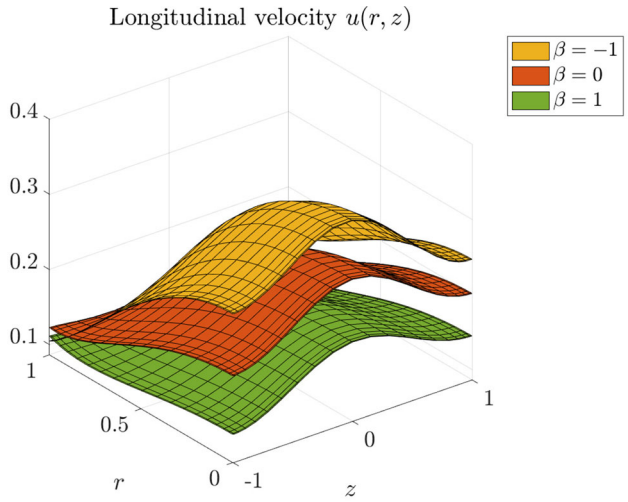


**Fig. 27** Wall profiles (59). Velocity $u(r,z)$, $\alpha=-1$, $\delta=1$, $\beta=-1,0,1$

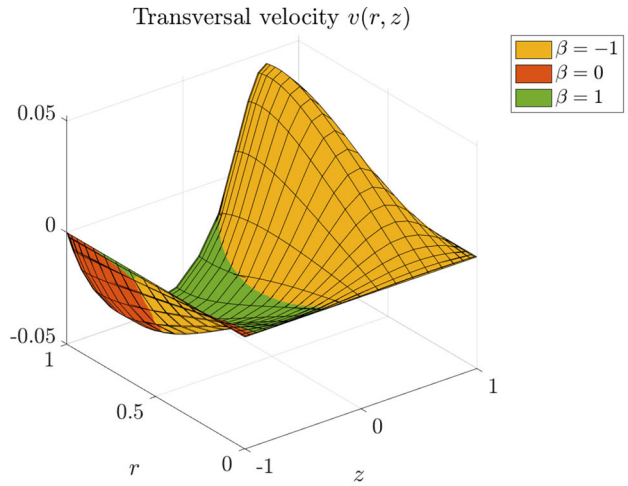


**Fig. 28** Wall profiles (59). Velocity $v(r,z)$, $\alpha=-1$, $\delta=1$, $\beta=-1,0,1$

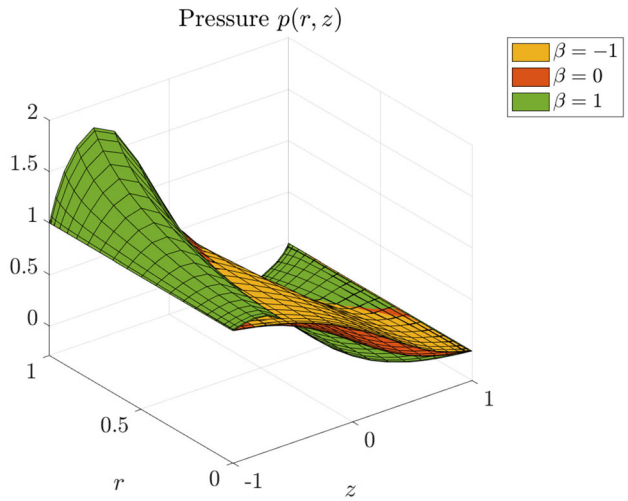


**Fig. 29** Wall profiles (59). Pressure $p(r,z)$, $\alpha=-1$, $\delta=1$, $\beta=-1,0,1$

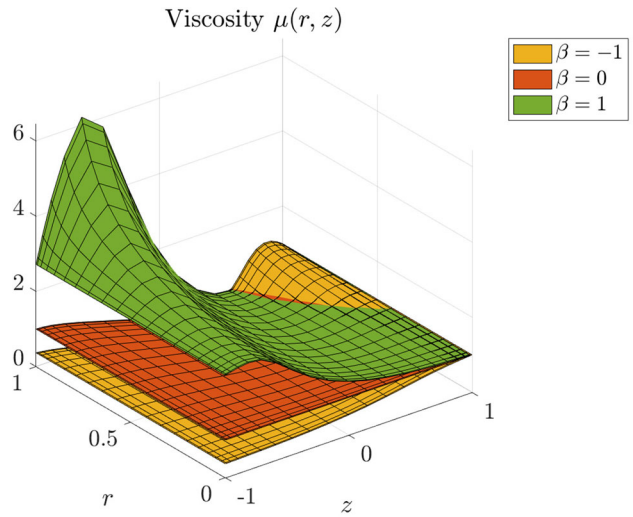


**Fig. 30** Wall profiles (59). Viscosity $\mu(r,z)$, $\alpha=-1$, $\delta=1$, $\beta=-1,0,1$

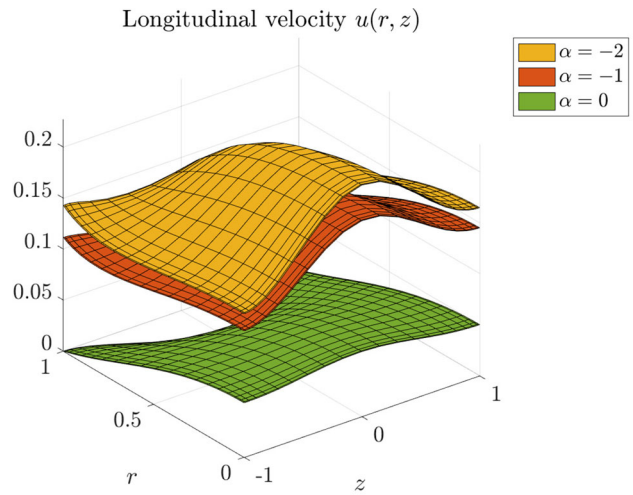


**Fig. 31** Wall profiles (59). Viscosity $\mu(r,z)$, $\beta=-1$, $\delta=1$, $\alpha=-2,-1,0$

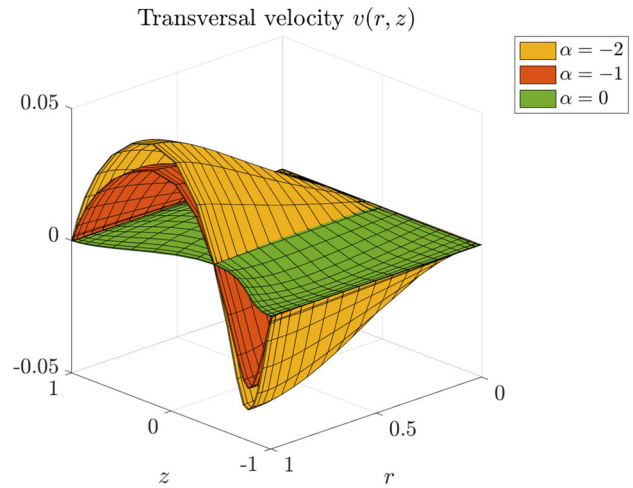


**Fig. 32** Wall profiles (59). Viscosity $\mu(r,z)$, $\beta=-1$, $\delta=1$, $\alpha=-2,-1,0$

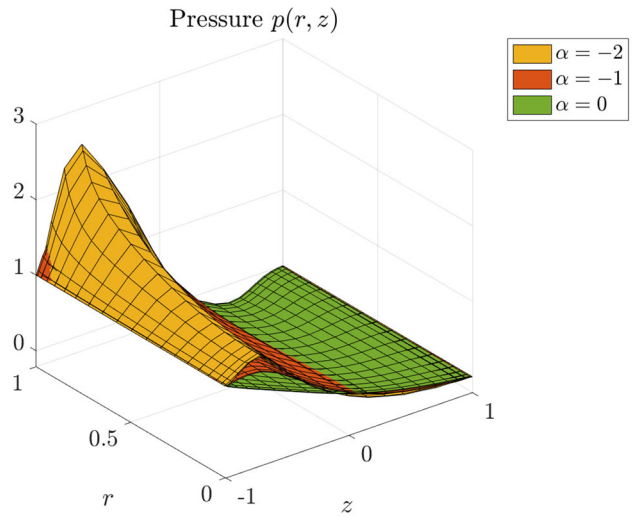


**Fig. 33** Wall profiles (59). Viscosity $\mu(r, z)$, $\beta = -1, \delta = 1, \alpha = -2, -1, 0$

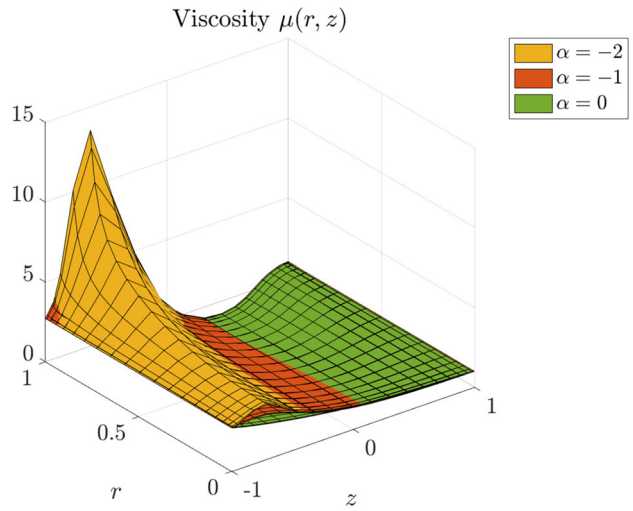


**Fig. 34** Wall profiles (59). Viscosity $\mu(r, z)$, $\beta = -1, \delta = 1, \alpha = -2, -1, 0$

Among possible extensions of the present paper, we mention the one in which one takes into account non steady inertial effects (we are currently working on this topic), i.e., the one in which the hypothesis of creeping flow is released. In this case the system becomes evolutive and acquires the extra nonlinearity due to the presence of the convective term in the linear momentum equation. Another interesting development would be to consider non linear rheological models, i.e., models in which the apparent viscosity depends on the pressure and also on the second invariant of the strain-rate tensor (power-law, viscoelastic, etc.).

**Acknowledgements** The present work has been performed under the auspices of the Italian National Group for Mathematical Physics (GNFM-Indam). This work has been done under the framework PRIN 2022 project "Mathematical modelling of heterogeneous systems" financed by the European Union—Next Generation EU, CUP B53D23009360006/B53D23009370006, Project Code 2022MKB7MM, PNRR M4.C2.1.1.

**Funding** Open access funding provided by Università degli Studi di Firenze within the CRUI-CARE Agreement.

## References


1. Bridgman, P.W.: The Physics of High Pressure. The Macmillan Company, New York (1931)
2. Stokes, G.G.: On the theories of the internal friction of fluids in motion, and of the equilibrium and motion of elastic solids (2007)
3. Barus, C.: Isothermals, isopiestics and isometrics relative to viscosity. Am J Sci **45**(266), 87–96 (1893)
4. Andrade, E.N.D.C.: Viscosity of liquids. Proc. R. Soc. Lond. Ser. A Math. Phys. Sci. **215**(1120), 36–43 (1952)
5. Denn, M.M.: Polymer Melt Processing: Foundations in Fluid Mechanics and Heat Transfer. Cambridge University Press, Cambridge (2008)
6. Rajagopal, K.: On implicit constitutive theories for fluids. J. Fluid Mech. **550**, 243–249 (2006)
7. Renardy, M.: Parallel shear flows of fluids with a pressure-dependent viscosity. J. Nonnewton. Fluid Mech. **114**(2–3), 229–236 (2003)
8. Johnson, K.L., Tevaarwerk, J.: Shear behaviour of elastohydrodynamic oil films. Proc R Soc Lond A Math Phys Sci **356**(1685), 215–236 (1977)
9. Johnson, K., Greenwood, J.: Thermal analysis of an Eyring fluid in elastohydrodynamic traction. Wear **61**(2), 353–374 (1980)
10. Gulik, P.: The linear pressure dependence of the viscosity at high densities. Physica A **256**(1–2), 39–56 (1998)
11. Singh, L.P., Issenmann, B., Caupin, F.: Pressure dependence of viscosity in supercooled water and a unified approach for thermodynamic and dynamic anomalies of water. Proc. Natl. Acad. Sci. **114**(17), 4312–4317 (2017)
12. Renardy, M.: Some remarks on the Navier–Stokes equations with a pressure-dependent viscosity. Commun. Partial Differ. Equ. **11**(7), 779–793 (1986)
13. Gazzola, F., et al.: On stationary Navier–Stokes equations with a pressure-dependent viscosity. In: REND. IST. LOMBARDO (SCIENZE) 128 (1994)
14. Gazzola, F.: A note on the evolution Navier–Stokes equations with a pressure-dependent viscosity. Z Angew Math Phys ZAMP **48**, 760–773 (1997)
15. Gazzola, F., Secchi, P.: Some Results on Stationary Navier–Stokes Equations with a Pressure Dependent Viscosity. Dip. di Matematica (1992)
16. Málek, J., Rajagopal, K.: Mathematical properties of the solutions to the equations governing the flow of fluids with pressure and shear rate dependent viscosities. Handb. Math. Fluid Dyn. **4**, 407–444 (2007)
17. Hron, J., Málek, J., Rajagopal, K.: Simple flows of fluids with pressure-dependent viscosities. Proc. R. Soc. Lond. Ser. A Math. Phys. Eng. Sci. **457**(2011), 1603–1622 (2001)
18. Kalogirou, A., Poyiadji, S., Georgiou, G.C.: Incompressible Poiseuille flows of Newtonian liquids with a pressure-dependent viscosity. J. Nonnewton. Fluid Mech. **166**(7–8), 413–419 (2011)
19. Fusi, L., Farina, A., Rosso, F.: Bingham flows with pressure-dependent rheological parameters. Int. J. Non-Linear Mech. **64**, 33–38 (2014)
20. Fusi, L., Farina, A., Rosso, F.: Mathematical models for fluids with pressure-dependent viscosity flowing in porous media. Int. J. Eng. Sci. **87**, 110–118 (2015)
21. Fusi, L., Farina, A., Saccomandi, G.: Buckley–Leverett equation with viscosities and relative permeabilities depending on pressure. SIAM J. Appl. Math. **75**(5), 1983–2000 (2015)
22. Fusi, L.: Non-isothermal flow of a Bingham fluid with pressure and temperature dependent viscosity. Meccanica **52**, 3577–3592 (2017)
23. Fusi, L., Rosso, F.: Creeping flow of a Herschel–Bulkley fluid with pressure-dependent material moduli. Eur. J. Appl. Math. **29**(2), 352–368 (2018)
24. Fusi, L.: Channel flow of viscoplastic fluids with pressure-dependent rheological parameters. Phys Fluids **30**(7) (2018)
25. Fusi, L.: Lubrication flow of a generalized Casson fluid with pressure-dependent rheological parameters. J. Nonnewton. Fluid Mech. **274**, 104199 (2019)
26. Zehra, I., Yousaf, M.M., Nadeem, S.: Numerical solutions of Williamson fluid with pressure dependent viscosity. Results Phys. **5**, 20–25 (2015)
27. Nakshatrala, K., Rajagopal, K.: A numerical study of fluids with pressure-dependent viscosity flowing through a rigid porous medium. Int. J. Numer. Methods Fluids **67**(3), 342–368 (2011)
28. Hron, J., Málek, J., Nečas, J., Rajagopal, K.: Numerical simulations and global existence of solutions of two-dimensional flows of fluids with pressure-and shear-dependent viscosities. Math. Comput. Simul. **61**(3–6), 297–315 (2003)
29. Fusi, L., Giovinetto, A.: A spectral collocation scheme for the two dimensional flow of a regularized viscoplastic fluid: numerical results and comparison with analytical solution. Math. Comput. Simul. (2024). https://doi.org/10.1016/j.matcom.2024.03.030